LA-UR- 08-6293

Approved for public release; distribution is unlimited.

Title: Report on 2D Richtmyer-Meshkov Instability Growth in Liquified Tin

Author(s): W. T. Buttler, G. Dimonte, Michael Furlanetto, J. E. Hammerberg, G. E. Hogan, F. Mariam, F. E. Merrill, C. Morris, P. Nedrow, Paulo Rigg, A. Saunders, C. L. Schwartz, Guillermo Terrones, and Michael Zellner

Intended for: C1 and C2 Report on RMI experiments at pRad.

Los Alamos
NATIONAL LABORATORY
EST. 1943

Los Alamos National Laboratory, an affirmative action/equal opportunity employer, is operated by the Los Alamos National Security, LLC for the National Nuclear Security Administration of the U.S. Department of Energy under contract DE-AC52-06NA25396. By acceptance of this article, the publisher recognizes that the U.S. Government retains a nonexclusive, royalty-free license to publish or reproduce the published form of this contribution, or to allow others to do so, for U.S. Government purposes. Los Alamos National Laboratory requests that the publisher identify this article as work performed under the auspices of the U.S. Department of Energy. Los Alamos National Laboratory strongly supports academic freedom and a researcher's right to publish; as an institution, however, the Laboratory does not endorse the viewpoint of a publication or guarantee its technical correctness.

Form 836 (7/06)

Report on 2D Richtmyer Meshkov Instability Growth in Liquified Tin

W. T. Buttler,[1] G. Dimonte,[2] Michael Furlanetto,[1] J. E. Hammerberg,[3] G. E. Hogan,[4] F. Mariam,[4] F. E. Merrill,[4] C. Morris,[4] P. Nedrow,[1] Paulo Rigg,[5] A. Saunders,[4] C. L. Schwartz,[4] Guillermo Terrones,[6] and Michael Zellner[1]
Los Alamos National Laboratory
[1] *Physics Division (P-23), MS H803*
[2] *Applied Physics Division (X-1), MS F699*
[3] *Applied Physics Division (X-1-SMMP), MS F699*
[4] *Physics Division (P-25), MS H846*
[5] *Dynamic and Energetic Materials Division (DE-9), MS P952*
[6] *Applied Physics Division (X-4), MS F699*
Los Alamos, NM 87545

In August 2008 we fielded two Richtmyer-Meshkov instability experiments at the LANSCE Proton Radiography Facility. The data were acquired by accelerating an Al flyer up to approximately 4.3 mm/μs toward a stationary Sn target. This flyer velocity yields a Sn pressure of $\approx$ 625 kbar just prior to shock-release at the free surface, and achieves a melt-on-shock of the Sn. The evolving systems were imaged with proton radiography to reveal instability bubble-and-spike growth-rate differences. One experiment was fielded in vacuum to baseline the dynamics, and the other was fielded in 5 bars ($\approx$ 5 atmospheres) of Xe to investigate particle transport.

I. INTRODUCTION

Los Alamos National Laboratory (LANL) is presently engaged in development and implementation of ejecta source term and transport models for integration into LANL hydrodynamic computer codes. Support of that effort spans a broad array of experimental activities, including ejecta source term measurements from machine roughened surfaces. The underlying postulate for ejecta formation is that ejecta are characterized by Richtmyer-Meshkov instability (RMI) phenomena. Because of that, a key element of the source modeling and transport centers on validation and verification RMI experiments, such as those presented here. In the RMI investigations, the material we have used is Sn, shocked by a supported wave from a Forest flyer. The flyer is launched to a velocity of $\approx 4.3 \pm 0.1$ mm/μs to cause a loading pressure sufficient to liquify the Sn on shock, which causes the surface perturbations to invert and form an RMI.

The first proton radiography (pRad) RMI experiment in 2005 was done with a small Sn target with an average thickness of 4 mm, and a diameter of 31.75 mm. The Sn surface was characterized by a sine wave of wavelength $\lambda = 2.5$ mm and amplitude $A = 0.2$ mm. An example of that target is seen in Fig. 1.

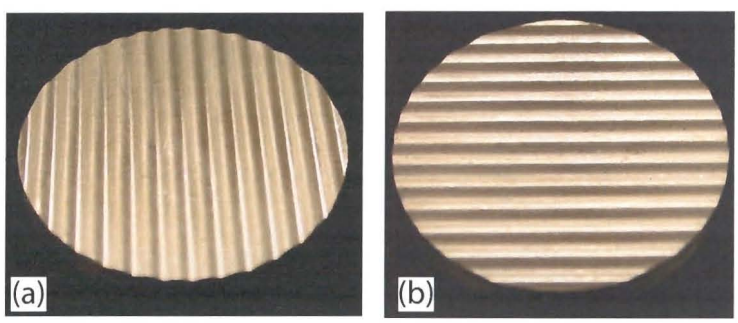

FIG. 1: These targets are made of annealed Sn. They were pressed first, annealed and cut to diameter and thickness. (The target manufacturing process was conceived and executed by Doug Landers, ISR-4; images courtesy of Robert Gallegos, P-23.)

The Forest flyer package (target assembly) for the initial experiment, with target, is shown schematically in Fig. 2. The target assembly was composed of a P089 HE lens (a 100 mm HE lens with its diameter reduced by machining), 1.5 inch thick PBX 9501 booster, a Forest flyer housing and an Al-6061 flyer. The flyer was diameter $d = 69.85$ mm, and thickness $\tau = 6$ mm. The Al flyer was positioned about 7 mm behind the PBX9501 booster. The HE gases expand into the volume between the booster and flyer and accelerate the flyer. The flyer accelerates until it impacts the target which is about 22 mm behind the target. The bottom of the target is mounted flush to the bottom of the phenolic holder so that on impact the flyer drives a shockwave into the Sn target, liquifying it on shock and causing

instabilities (RMIs) to form on the backside as the shockwave releases to vacuum.

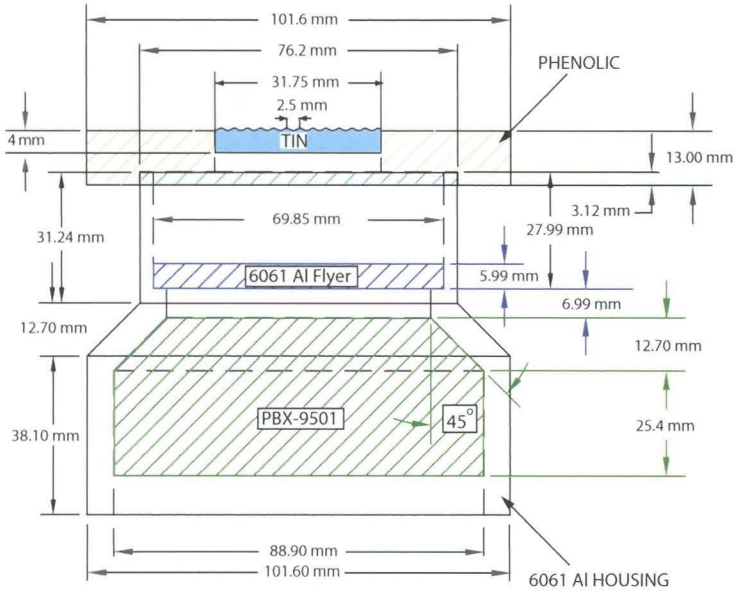

FIG. 2: This figure shows the Forest flyer package with the target, PBX-9501 HE Booster, Target holder, and Forest flyer housing. The dimensions of each are shown. Not shown is the P100 lens which must be cut down to a diameter of < 88.9 mm to allow it to mate with the booster charge.

The resulting instabilities were proton radiographed, with those results presented in Fig. 3. Prior to the experiment, Rob Hixson calculated that the flyer velocity should have been $u_{calc} = 4.1 \pm 0.1$ mm/μs, based on this HE-Lens and PBX 9501 booster configuration. The pRad images indicate a flyer velocity at impact of $u_{flyer} = 4.3 \pm 0.3$ mm/μs. This value is arrived at by considering all images of the flyer in flight, and fitting both the front and back of the in-flight-flyer position as a function of time, and considering that the flyer impacted the target prior to the third frame in Fig. 3. The pRad flyer velocity calculation included 2 images not seen in this short time series, but included in the general data release. In addition, subsequent hydrodynamic calculations performed in P-23 estimate a flyer velocity of 4.0 mm/μs, and X-Division calculations approximate this velocity as 3.9 mm/μs.

From the RMI image analysis, the difference between the bubble- and spike-growth rate was calculated from the data and seen to be linear: $\Delta u_{b-s} = 1.55$ mm/μs. The calculation estimated the bubble position once it was clearly resolved within the images. The bubble is traveling at $u_b = 3.142$ mm/μs, and the spike is traveling at $u_s = 4.692$ mm/μs, in the pRad rest frame, as determined by linear regression. A particle velocity calculation, based on the flyer velocity, gives an estimated free surface velocity of $u_{fs} \approx 3.4$ mm/μs, a value larger than u_b and smaller than u_s, as expected from RMI theory.

Figure 4 shows an AWE calculation of the target assembly described by Fig. 2. Their model does not include the HE, but considers an Al flyer impacting the target at about 4.2 mm/μs. They have since improved their results and presented them at conferences and JOWOGs.

A particular feature of single-mode RMI theory is that the spike-tips will not break off to form ejecta in vacuum. Of course, this theoretical RMI result is incorrect as it neglects surface tension, but given the time (field of view) over which the pRad facility can provide dynamic images it is not possible to observe the breakup with the parameters of the initial experiment. Because of this, the experiments were redesigned to incorporate multiple sinusoidal-mode features on a single Sn target in an effort to capture bubble-merger, and, consequently, spike-breakup. Also of interest was to observe and model transport of the features into a high pressure atmosphere of 5 bar Xe.

The new package design also focussed on suppression of the "cuped" region that tends to obscure the instability features in the data (see Fig. 3). The *cup* is a symmetric feature that surrounds the target and forms as the target splashes on the edges from the shock and Al flyer impact, and shock releases in the material. The velocity of the cup leading edge is comparable to the spike-tip growth rates.

In an effort to determine a package geometry that would inhibit the cupping effect, new package concepts were informed through hydrodynamic modeling with CTH, an Eulerian based shockwave continuum mechanics code developed at Sandia National Laboratory. The resulting final package is seen in Fig. 5. For package simulations, a SESAME equation of state (EOS) and Steinberg-Guinan-Lund (ST) material strength model were used for the Al 6061, a Mie-Gruneisen EOS and a ST strength model were used for the Sn, a Mie-Gruneisen EOS with density variations and a ST strength model were used for the Polyurethane foam, an ideal gas EOS was used for the Neon gas,

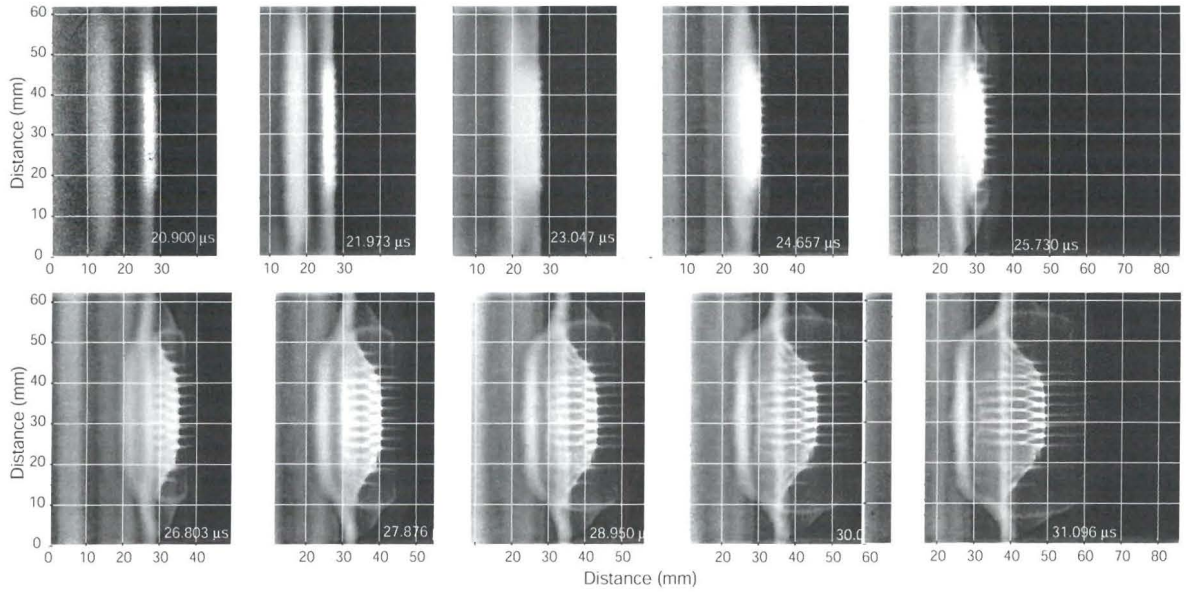

FIG. 3: These images show the pRad time-sequence of the flyer and target prior to impact, as well as the RM instability growth after impact. The first three images are of low resolution and mainly show the Al impactor in flight and up to impact with the Sn target. The final images show the shock wave and RM instability evolution and instability growth. The images are nominally separated in time by 1-1.3 μs. (These images were processed by Cynthia Schwartz, P-25.)

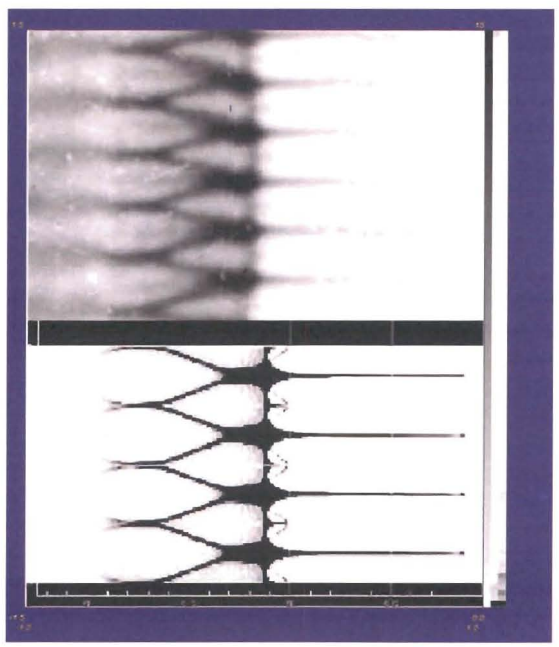

FIG. 4: These images compare calculation by AWE with experimental pRad data. The calculation was done by David Youngs, Brian Grieve and Robin Williams.

a Mie-Gruneisen EOS was used for the acrylic, and Jones-Wilkins-Lee (JWL) EOSs were used for the PBX 9501 and TNT high explosives. Additionally, the sinusoidally perturbed Sn targets were replaced with pristine slabs of Sn to focusing the modeling efforts on package/shockwave interactions and not on growth of the instabilities.

Figure 6 shows a falsely colored radiograph of the 2005 experiment and Fig. 7 a corresponding CTH calculation of material coordinates (not a model of the radiographic attenuation). The CTH model closely predicts the Al flyer velocity, 4.0 km/s vs. 4.3 km/s experimental, and Sn target free-surface velocity, 3.2 km/s vs. 3.4 km/s. Additionally,

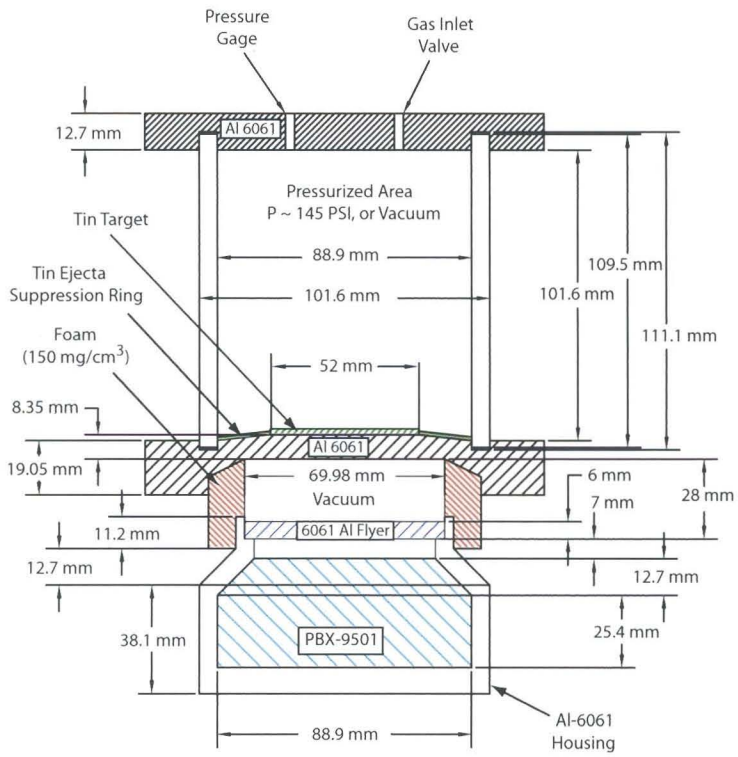

FIG. 5: This figure shows the modified Forest flyer package with the target, PBX-9501 HE booster, target holder, and Forest flyer housing. The dimensions of each are shown. Not shown is the P100 lens which must be cut down to a diameter of < 88.9 mm to allow it to mate with the booster charge.

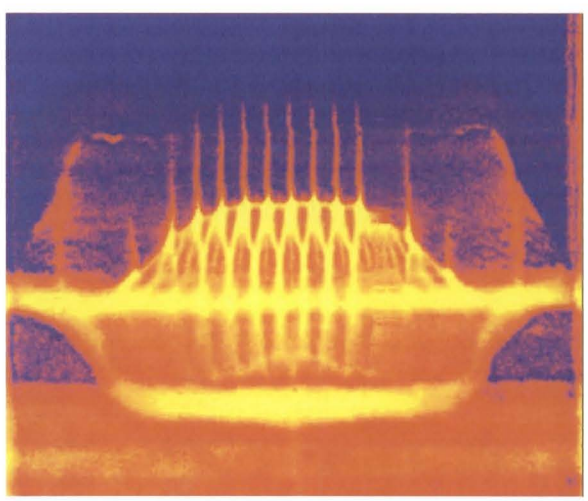

FIG. 6: Falsely colored image of the Forest flyer/Sn system shot into vacuum.

CTH appears to predict the ejecta cup produced from shockwave release at the Al holder free-surface.

Figure 8 shows a CTH calculation of the current package design, which includes addition ~~of a~~ raised target baseplate with beveled sides and a diamond turned Sn ring (colored green). The combination of these features was predicted by CTH to suppress the problematic ejecta. Comparison of Fig. 8 with the corresponding 2008 experimental radiograph, Fig. 10, indicates that the modifications were successful.

A second experimental feature captured in the CTH modeling, both in the previous (2005) and the most recent experiments, is curvature of the target free-surface. This curvature is troublesome because it complicates the analysis

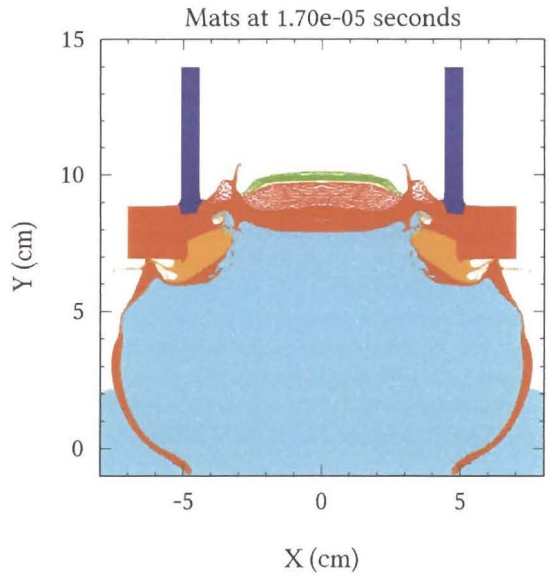

FIG. 7: 2-D cylindrical geometry CTH calculation for the 2005 Forest flyer/Sn system shot into vacuum.

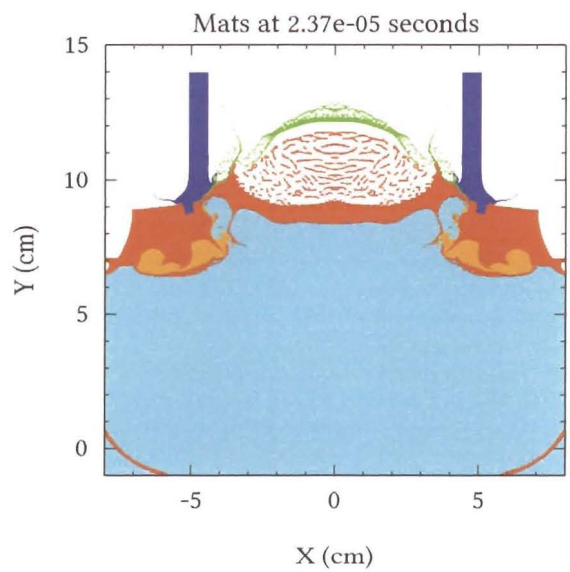

FIG. 8: 2-D cylindrical geometry CTH calculation for the current Forest flyer/Sn system shot into Neon.

of the instabilities. In upcoming experiments, CTH will be used to assist in the design of a forrest flyer/package/target system, possibly through addition of momentum traps or redesign the flyer shape, to eliminate the reflecting waves that cause the curvature.

The target for the 2008 experimental series was based on half-angles observed in machine finishes on Sn where the average surface roughness was $R_a = 32$ μin. (≈ 3.2 μm peak-to-peak). In different 32 μin. samples, half-angles between 75° to 88° were observed when different machine tools were used. This approach led to a Sn target of diameter $d = 52$ mm, with three target regions of fixed wavelengths of $\lambda = 1.2$, 1.8, and 2.7 mm. These three regions had a fixed amplitude of $A = 0.1$ mm and were separated by two regions of fixed wavelength and varying amplitude. This resulted in a target where two sections joined two half-wavelengths of varying similar amplitude and varying wavelength, i.e., a region with $A = 0.1$ mm and $\lambda = 1.2$ mm joined a region with $\lambda = 1.8$ mm with varying amplitude that then joined a region of $A = 0.1$ mm and $\lambda = 2.7$ mm. On the other side of the target, two regions of $A = 0.1$ mm

and $\lambda = 1.2$ and 1.8 mm were joined by a region of $\lambda = 1.2$ mm and varying amplitude. The surface perturbations are presented in Fig. I. The target thickness was nominally a maximum of 2.1 mm and a minimum of 1.9 mm. The target was placed on top of the Forest flyer package as depicted in Fig. 5, and was surrounded by the ejecta suppression ring that was 1 mm thick Sn to impedance match with the Sn target.

Two packages with targets described above were fielded at pRad in August 2008. One package was fielded in vacuum and the other in 5 bar Xe. The vacuum experiment is to be used for code V&V, and the other in support of transport model development. The Atomic Weapons Establishment continues to assist in modeling these data, and Guillermo Terrones of LANL is as well.

Eighteen of the pRad images from the Xe experiment are presented in Fig. 10. There were a total of twenty two images acquired, indicating that four images are omitted. The images omitted were from times 0.0, 2.0, 10.0, and 26.0 μs. The images at times 0.0 and 2.0 μs are static, as was the best static image at time 1.0 μs. The flyer impacted the target mount that includes 8.3 mm of Al-6061, either just prior to, or just after, 9.0 μs (last image in the upper row of Fig. 10), so the image at 10.0 μs was omitted as it was essentially static as well. The 26.0 μs image was omitted for figure brevity.

From the data, we can approximate several important parameters, including the velocity of the flyer at impact with the target mount, the velocity of the leading edge of the instability interactions with the Xe gas, and the bubble velocities. We can also approximate the Xe shock wave velocity based on the jump velocity of the flyer into the gas through use of 1D piston approximations.

The leading edge of the flyer is approximately $z = 10.3$, 16.1, 23.9, 26.9, and 30.8 mm. The relevant times for these positions are $t = 2$, 3, 5, 7, and 9 μs. If all these times and positions are used, the resulting flyer velocity at impact is $u_{flyer} \approx 3.95$ mm/μs. If four of the times and positions are used the resulting flyer velocity at impact is $u_{flyer} \approx 4.05$ mm/μs. These results are based on the assumption that the static position of the flyer is $z_0 \approx 9.4$ mm, the position of the target mount is 22 mm beyond this position, and a quadratic fit to the data; the results are preliminary, i.e., more careful analysis may lead to a different result. However, we note that this flyer velocity is consistent with modern hydrodynamic modeling and the first experimental results. We also note that this flyer velocity leads to a gas-shockwave velocity of about 4.0 mm/μs in 5 bar Xe.

In a similar manner we extracted the bubble and spike velocities in the center of the target, and around 32- and

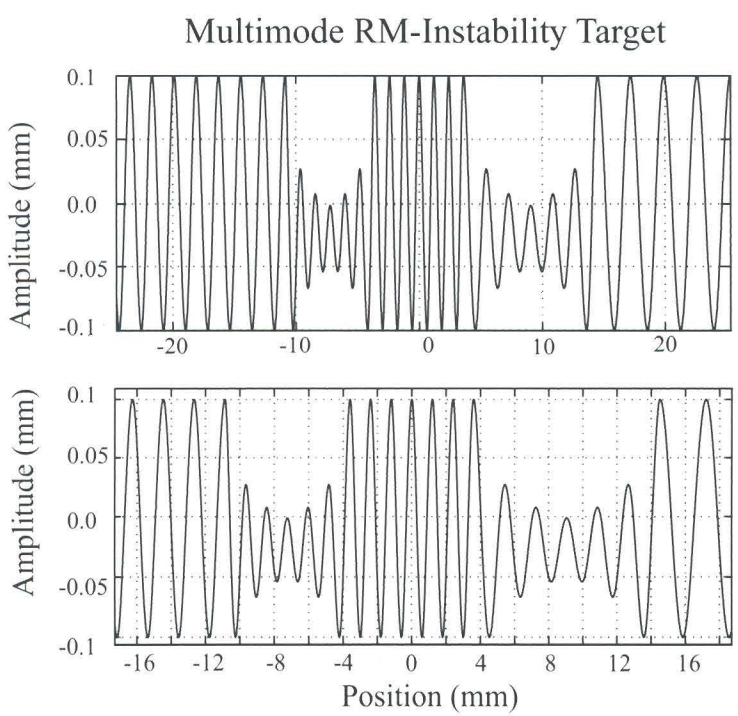

FIG. 9: This pattern illustrates the MM sinusoidal target. The surface was machined diamond machined on a 4-axis mill to a mirror like finish (diamond turn finish). The bottom of the targets was machined to a roughness of $R_a = 16$ μin. finish and epoxied to the Al 6061 surface as shown in Fig. 5.

68-mm in the vertical dimension of the target system. Those results are presented in Fig. 11. Considering the central spike velocities, they immediately jump to $u_{spike} \approx 4.1$ mm/μs and smoothly decrease to $u_{spike} \approx 3.3$ mm/μs over the experimental duration of about 15 μs. The outer wings begin at $u_{spike} \approx 3.6$ mm/μs and decrease smoothly to $u_{spike} \approx 3.2$ mm/μs. This spike time velocity decrease is attributable to particle drag. Also evident in the images is a redistribution of the Sn mass within the mix layer and folding and mushrooming of the spike tips in the gas.

The bubble velocities behave similarly, with the central bubble velocities at $u_{bubble} \approx 3.4$ mm/μs which then smoothly decreases to $u_{bubble} \approx 3.1$ mm/μs. The bubble velocities in the wings begin at $u_{bubble} \approx 2.9$ mm/μs which then smoothly decreases to $u_{bubble} \approx 2.6$ mm/μs. Again, these results are preliminary. The central results should be compared with the expected free-surface jump velocity of $ufs \approx 3.4$ mm/μs. We note that we have only included the RMI experiment into Xe. The other data into vacuum are being processed further.

In conclusion, we learned much from these experiments to inform future work. Specifically, we note that these experiments were performed with the pRad $-I$ lens. We discovered that we can use the $\times 3$ magnifier if we diagnose the flyer velocity through use of multiple Doppler velocimetry probes. The probes would protrude through the target mounting plate, near the edges, and would provide the initial conditions for flyer impact. The $\times 3$ magnifier would reduce our field of view to about 40 mm in each direction, but it would also allow us to scale the surface features down near 0.4 mm in wavelength and 1/30 mm in amplitude, and still resolve the dynamic features at pRad. This would give a surface feature scale about $\times 10$ the feature scales of machined surface of roughness $R_a = 32$ μin. At these scales, it is likely that we can take a lineout from a real surface finish, scale it up by a factor of ten, and machine that 2D feature onto a Sn target with the MST-7 4-axis milling machine. The features would be highly multi-mode in nature and would like breakup over the time periods of a 40 mm travel distance, or about 15 μs. This is the future direction of this effort, into vacuum and into gas.

Acknowledgments

This work was supported by the United States Department of Energy.

The collaboration includes Robin Williams, Brian Grieves and David Youngs of the Atomic Weapons Establishment.

We gratefully acknowledge the contributions to these experiments by Patrick T. Reardon and Felix P. Garcia of MST-7. Felix machined the surface perturbations on the RMI targets in the 2008 experimental series.

All images were processed extensively by either Cynthia L. Schwartz or Chris Morris and William Buttler. The analysis for the first experiment was a collaboration between Schwartz, Morris and Buttler. The Xe RMI data were analyzed by Buttler and Morris.

The final experiment design was a engineered by William Buttler and Jim Hammerberg.

In both sets of experiments, the most important part was the target. We were frustrated at every turn to get quality targets for the first RMI series until Doug Landers (ISR-4) developed a technique to get us the targets we needed. The targets for the second series were machined by Felix Garcia on the MST-7 4-axis machine.

Finally, the pRad team is extensive. These guys have incredible breadth and talent. Cheers to them all for an outstanding data set! It is likely that someone's name was left off inadvertently. Regrets in advance.

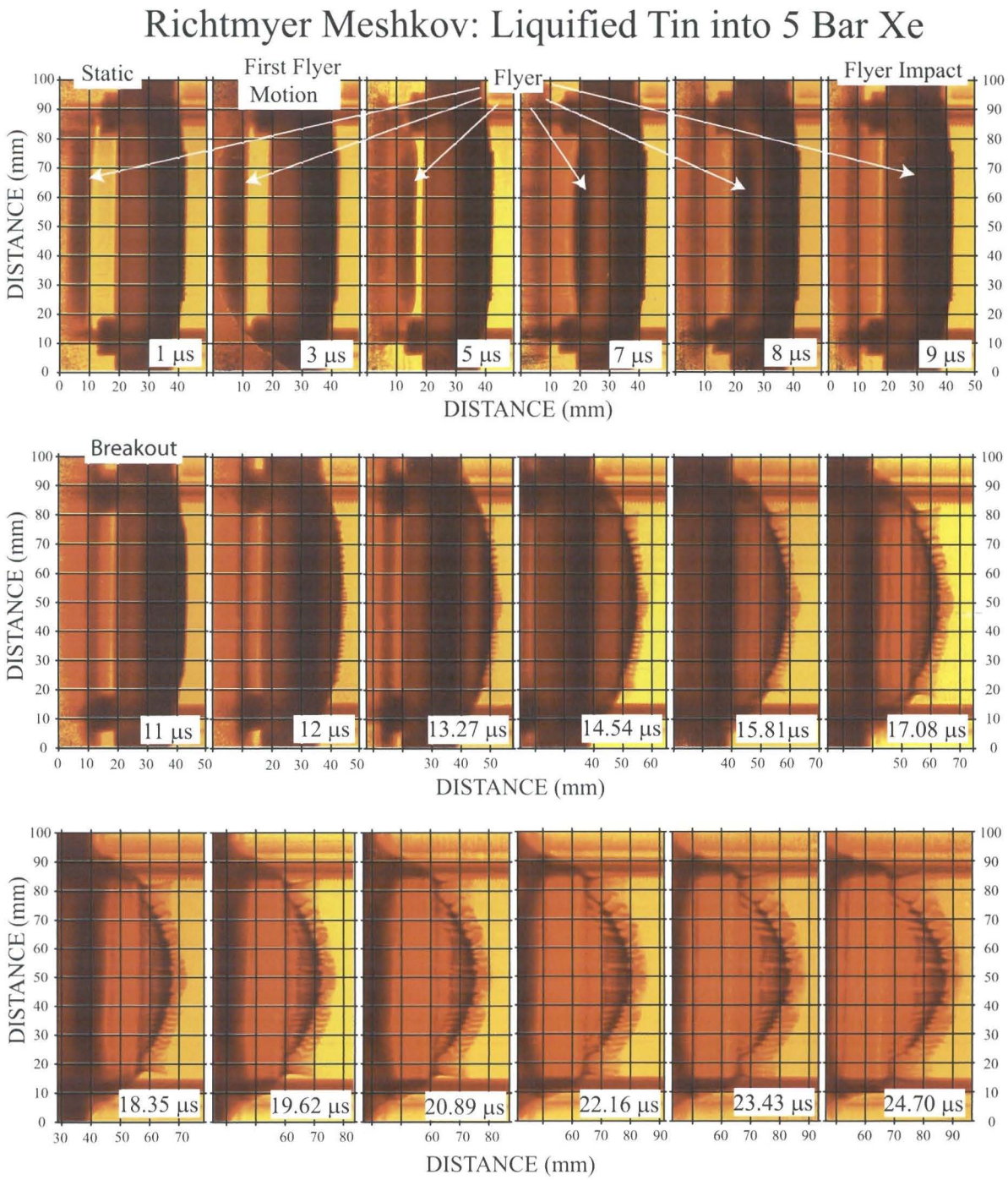

FIG. 10: These RMI proton radiography data were acquired at the pRad facility in August 2008. The acquisition time of each image is shown at the bottom of each. The upper row of images show the evolution of the Al-6061 flyer from its static position until impact with the Al-6061 target mount. The flyer is $\tau = 6$ mm and the target mount is $\tau = 8.35$ mm thick (see Fig. 5).

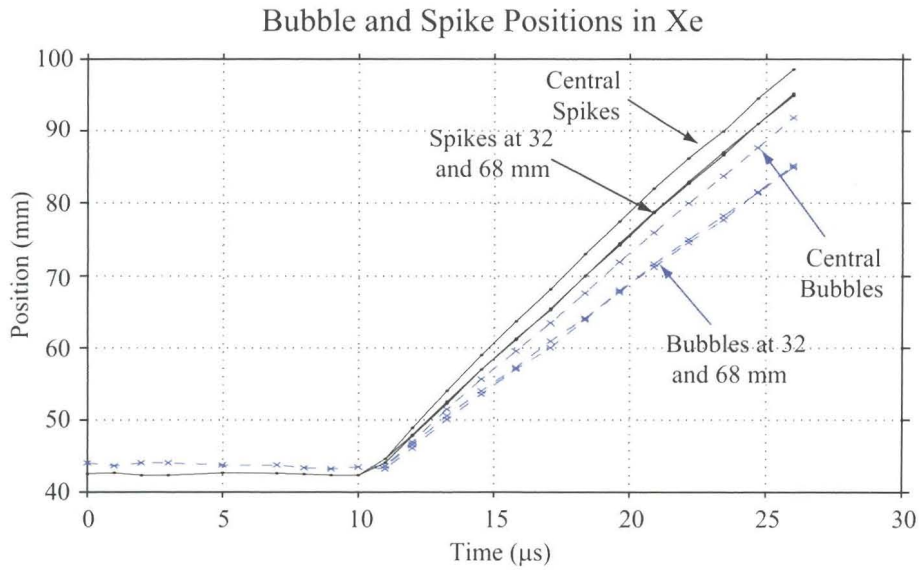

FIG. 11: The bubble and spike positions invert at shock breakout, thus the blue and black lines cross each other. The uppermost solid black line is the central spike positions versus time, and the uppermost blue dashed line is the central bubble positions. The velocities decrease slightly with time.